frontiers | Frontiers in Marine Science

TYPE Original Research
PUBLISHED 31 October 2023
DOI 10.3389/fmars.2023.1254410

OPEN ACCESS

EDITED BY
Fei Han,
University of New Hampshire, United States

REVIEWED BY
Shengxiong Yang,
Guangzhou Marine Geological Survey, China
Jinxiu Yang,
China University of Petroleum, China
Duanxin Chen,
Chinese Academy of Sciences (CAS), China
Jiangxin Chen,
Qingdao Institute of Marine Geology (QIMG), China

*CORRESPONDENCE
Cong Cheng
ccheng2017@cug.edu.cn
Tao Jiang
taojiang@cug.edu.cn

RECEIVED 07 July 2023
ACCEPTED 18 October 2023
PUBLISHED 31 October 2023

CITATION
Ren J, Cheng C, Jiang T, Kuang Z, Lai H, Liang J, Chen Z and Li T (2023) Faults and gas chimneys jointly dominate the gas hydrate accumulation in the Shenhu Area, northern South China Sea.
Front. Mar. Sci. 10:1254410.
doi: 10.3389/fmars.2023.1254410

Faults and gas chimneys jointly dominate the gas hydrate accumulation in the Shenhu Area, northern South China Sea

Jinfeng Ren[1], Cong Cheng[2,3]*, Tao Jiang[2,3]*, Zenggui Kuang[1], Hongfei Lai[1], Jinqiang Liang[1], Zigui Chen[3] and Tao Li[3]

[1]National Engineering Research Center of Gas Hydrate Exploration and Development, Guangzhou Marine Geological Survey, China Geological Survey, Ministry of Natural Resources, Guangzhou, China, [2]Institute for Advanced Marine Research, China University of Geosciences, Guangzhou, China, [3]Hubei Key Laboratory of Marine Geological Resources, China University of Geosciences, Wuhan, China

Gas hydrates possess significant potential as an energy resource and exert a notable influence on global climate change. The Shenhu Area is one of the globally recognized focal points for gas hydrate research, and additional investigation is required to fully comprehend its gas migration mechanism. By utilizing the most recent core-log-seismic data and gas geochemical data, a comprehensive analysis was conducted to determine the influence of gas migration pathways on gas hydrate accumulation in the study area. This study investigated the various types of gas migration pathways, employing integrated geological models that incorporate faults and gas chimneys to understand their respective contributions to the accumulation of gas hydrates. Based on these findings and drilling constraints, a three-gas combined production model was subsequently proposed. Thermogenic gas, secondary microbial gas, and *in situ* microbial gas are all potential sources of the gas responsible for hydrate formation. Thermogenic gas plays a significant role in the gas hydrate system, as evidenced by distinct features of late-mature thermogenic gas observed in gas samples extracted from hydrates in Well W18. In the study area, the primary conduits for gas migration encompass deep faults, branch faults, and gas chimneys. Among these, deep faults act as the most crucial pathways of thermogenic gas migration. The integration of geological models that incorporating deep faults and gas chimneys has profoundly impacted the accumulation of gas hydrates in the Shenhu Area, consequently influencing the distribution of shallow gas and gas hydrate. Furthermore, the proposed three-gas combined production model, which involves the simultaneous extraction of deep gas reservoirs, shallow gas reservoirs, and gas hydrates, holds significant implications for exploring and developing deep-water natural gas resources. However, its successful implementation necessitates interdisciplinary collaboration among scientists.

KEYWORDS

gas hydrates, faults, gas chimneys, shallow gas, gas origin, gas migration, Shenhu Area

1 Introduction

Gas hydrates are solid compounds with cage structures, which have attracted worldwide attention due to their huge energy resource potential (Kvenvolden, 1993; Dickens et al., 1995; Sloan, 2003; Milkov, 2004; Solomon et al., 2007). Scientists estimate that the global reserves of gas hydrate resources are approximately 3×10^3 trillion cubic meters of methane (Boswell and Collett, 2011). These vast reserves hold immense potential as a viable alternative energy source for humanity in the coming years. In recent decades, several nations, including Russia, Canada, the United States, Japan, and China, have conducted production tests on gas hydrates (Makogon et al., 2007; Beaudoin et al., 2014; Chong et al., 2016; You et al., 2019; Ouchi et al., 2021; Yu et al., 2021). These production tests signify substantial progress toward the commercial utilization and extraction of this valuable resource.

The formation and accumulation of gas hydrates are influenced by a multitude of factors, encompassing the origin and migration of gas, the characteristics of reservoirs, as well as pressure and temperature conditions (Collett et al., 2009). Extensive research has demonstrated that the formation of hydrates necessitates the ingress of gas with a high flux into the gas hydrate stability zone (GHSZ), which cannot be largely fulfilled by *in situ* microbial gas (Kuang et al., 2018; Lai et al., 2023). Consequently, the importance of deep thermogenic gas as a crucial gas source for gas hydrate accumulation becomes apparent. Additionally, the study of gas migration pathways has emerged as an essential aspect of gas hydrate systems, obtaining considerable attention from researchers (Davies et al., 2014; Fu et al., 2020; Santra et al., 2022). Gas hydrates are predominantly found on continental margins across the globe. In marine environments, the accumulation of gas hydrates is intricately associated with faults, acting as vital conduits for the migration of deep thermogenic gas into the GHSZ (Milkov and Sassen, 2002; Hui et al., 2016). Moreover, the pathways for gas migration include both vertical transport conduits, such as gas chimneys and mud diapirs, and lateral migration pathways, such as high-permeability sand layers (Fraser et al., 2016; Hillman et al., 2017; Su et al., 2017; Ren et al., 2022; Slowey et al., 2022; Zhang et al., 2023). These pathways are essential components that should not be overlooked or disregarded.

The Shenhu Area in the South China Sea stands out as a prominent hotspot for gas hydrate research worldwide (Figure 1A). Notably, two rounds of successful production tests have already been conducted in this region (Li et al., 2018; Qin et al., 2020; Ye et al., 2020; Qin et al., 2022). A series of drilling expeditions in the Shenhu Area has led to notable breakthroughs in understanding the gas hydrate accumulation mechanism. These endeavors have contributed to significant advancements in research within the region. The formation of hydrates has been found to be significantly influenced by deep thermogenic gas (Zhang et al., 2017; Wang et al., 2021; Lai et al., 2022; Liang et al., 2022). Therefore, the transportation of deep thermogenic gas to shallow strata has come out as a topic of scholarly interest. Seismic data analysis revealed that gas chimneys and mud diapirs are the primary conduits for vertical gas migration. Additionally, polygonal faults have been identified as another contributing factor in the process (Chen et al., 2013; Liang et al., 2017; Su et al., 2017). Due to the earlier acquisition time of seismic data, deep reflections could be more explicit, and a large number of fuzzy zones on seismic profiles can be observed. In order to further enhance the understanding of gas hydrates in the Shenhu Area, the Guangzhou Marine Geological Survey (GMGS) undertook the acquisition of high-resolution 3D seismic data in 2018. Cheng et al. (2020) described the characteristics of various types of gas chimneys. Their proposal suggests that gas chimneys, originating from the Paleogene and terminating in the Quaternary, play a pivotal role in facilitating the accumulation of gas hydrates. Zhang et al. (2023) proposed that the large sediment thickness at the ridge of the canyons led to gas chimney formation. Additionally, deep faults serve as crucial conduits for the vertical migration of thermogenic gas (Jin et al., 2020; Wang et al., 2021). Nevertheless, the significance of faults, particularly their relationship with gas chimneys, needs to be more frequently discussed in the gas hydrate accumulation process.

In 2020, the GMGS carried out a reprocessing of seismic data, leading to enhanced visualization of deep faults. In this study, the up-to-date core-log-seismic data and gas geochemical data were employed to comprehensively explore and analyze the role of faults in the gas migration process. The study also investigated their contribution to gas hydrate accumulation alongside gas chimneys. We characterized the gas hydrate occurrence of seven drillings and the coupled geological models of faults and gas chimneys under the constraints of these drillings. Subsequently, we elucidated various gas migration pathways, including deep faults, branch faults, and gas chimneys. Combined with gas geochemical data, we found evidence that deep thermogenic gas is an essential gas hydrate source. Then, this paper clarified the contribution of different geological models to gas hydrate accumulation. Finally, a three-gas combined production model of deep natural gas reservoirs, shallow gas reservoirs, and gas hydrates was proposed to promote the exploration and development of offshore oil and gas resources.

2 Geological setting

The Shenhu Area can be found in the northern region of the South China Sea, and it is structurally situated within the Baiyun Sag of the Pearl River Mouth Basin (Figures 1A, C). It is worth noting that the significant LW3-1 gas field was successfully discovered within this area. In the northern South China Sea, the Pearl River Mouth Basin encompasses a vast expanse and holds the distinction of being the largest petroleum-rich basin (Zhu et al., 2009; He et al., 2017; Zhang et al., 2021b). Over the course of the Cenozoic era, the basin has experienced numerous instances of tectonic activity, leading to the emergence of a diverse range of faults, diapirs, and gas chimneys (Figure 1B) (Sun et al., 2008; Shi et al., 2014; Pang et al., 2018; Sun et al., 2019). The presence of these geological features has fostered favorable conditions for the flow of fluids. The predominant sedimentary deposits within the basin are characterized by the lacustrine facies of the Wenchang and Enping

Formations. These formations are widely acknowledged as the key hydrocarbon source rocks within the region. The transitional facies of the Zhuhai Formation may also serve as source rocks. The basin comprises diverse facies, ranging from littoral to bathyal and abyssal environments. These facies include the Zhujiang, Hanjiang, Yuehai, and Wanshan Formations, alongside the Quaternary strata (Mi et al., 2018; Zhang et al., 2021a). The sediment thickness of the Cenozoic strata in the Baiyun Sag can reach about 8 km, showing good hydrocarbon generation conditions (Zhu et al., 2021).

The study area is characterized by water depths ranging from 500 to 1700 m (Figures 1A, C). Furthermore, it holds the distinction of being the pioneering pilot test area for the exploration and exploitation of gas hydrates in the South China Sea, and production tests were successfully carried out in 2017 and 2020. The evidence of favorable conditions for gas hydrate accumulation in this area is compelling. Furthermore, it is noteworthy that the LW3-1 gas field is situated within a proximity of less than 10 km from the study area. The close proximity of the area strongly indicates the existence of substantial thermogenic gas reserves in deep formations, thus presenting a promising potential as a viable source for gas hydrate accumulation (Figure 1C) (Zhu et al., 2009).

3 Data and methods

3.1 Core-log-seismic data

The research employed 3D seismic data predominantly collected in 2018, covering an estimated expanse of 800 km^2. In 2020, the GMGS undertook data reprocessing, with a particular focus on deep reflection structures. The specific parameters of the seismic data and the processing procedures can be found in Cheng et al. (2020). Based on the seismic data and previous research, the sequence stratigraphic framework was established (Shi et al., 2014; He et al., 2017). In addition, Geoframe® software was used to extract seismic attributes like coherence slices, and then characterize the planform distribution of faults and gas chimneys.

In 2007, 2015, and 2018, logging data from seven wells, namely SH5, W22, W17, W07, W18, SH2, and W11, were obtained and processed by Schlumberger® (Figure 1C). The logging techniques employed included GR logging, RES logging, Vp logging, density (DEN) logging, and resistivity imaging (RES_BD_IMG) logging. These methodologies mainly aimed to detect gas hydrates and free gas, as illustrated in Figure 2 (Collett et al., 2019; Cook et al., 2023). However, due to the limited coring wells, a small number of cores were obtained from Well W17, and a comprehensive observation and description of each segmented core was conducted.

3.2 Gas geochemical data

Although well logs at seven wells were acquired, only some wells were tested for gas geochemistry (Table 1). Among them, hydrate gas samples of Wells W17, W18, and W11 were obtained (Zhang et al., 2019), hydrate gas samples of SC-1, SC-2, SC-W01B, SC-W01C, SC-W02B, SC-W03B, SC-2017, SC-2020, and samples from the LW3-1 natural gas reservoirs were also used for comparisons (Lai et al., 2022; Liang et al., 2022). Gas geochemical data mainly include methane carbon isotope composition ($\delta^{13}C\text{-}C_1$), the ratio of methane to the sum of ethane and propane ($R=C_1/(C_2+C_3)$), and methane hydrogen isotope composition ($\delta^{2}H\text{-}C_1$), which are all used to identify the source of gas (Milkov and Etiope, 2018).

3.3 History of fault activity

Based on the high-resolution seismic data, this work selected a few typical faults to analyze their activity history, which mainly includes the sedimentary thickness of the hanging wall and footwall of faults in each sedimentary period, fault expansion index, and fault activity rate (Jackson and Rotevatn, 2013; Zhao et al., 2016). The sedimentary thickness was first measured by the two-way travel time (TWT) and then converted into depth according to the time-depth transformation formula (Zhou et al., 2009). The expansion index is the ratio of the sedimentary thickness of the hanging wall of the fault to the sedimentary thickness of the footwall, which is used to indicate whether the fault is active. The fault activity rate is the difference in sedimentary thickness between the hanging wall and the footwall during a certain sedimentary period.

4 Results

4.1 Gas hydrate occurrence

Only logging data, including the GR curve, RES curve, and Vp curve, were obtained at Well SH5 (Figure 2A). Among them, the RES curve value exhibits minor variation, and no evident presence of gas hydrates or free gas was observed (Supplementary Data Sheet 1).

The geographical location of Well W22 is situated on the eastern side of Well SH5 (Figure 1C). At approximately 186.1 to 190 mbsf, there is an observed increase in the values of both the RES curve and Vp curve, accompanied by the highlighting of the RES_BD_IMG (Figure 2B). Taken together, these observations strongly indicate the gas hydrate occurrences (Supplementary Data Sheet 1).

The values of the RES curve and Vp curve increase sharply between ~210 mbsf to ~260 mbsf of Well W17, and the RES_BD_IMG also show highlighted features, demonstrating the gas hydrate occurrences (Figure 2C). The honeycomb structures formed by gas hydrate dissociation are also visible on cores. The gas hydrate layer exhibits an effective thickness of approximately 43.1 m, with an average gas hydrate saturation of approximately 19.4% (Supplementary Data Sheet 1). Beneath the gas hydrate layer, there is a noticeable increase in the RES curve value, indicating the presence of a free gas layer. However, the Vp value decreases within this layer.

Well W07 is situated on the ridge of the canyon in the northern region of the study area (Figure 1C). Around 150 mbsf, the RES

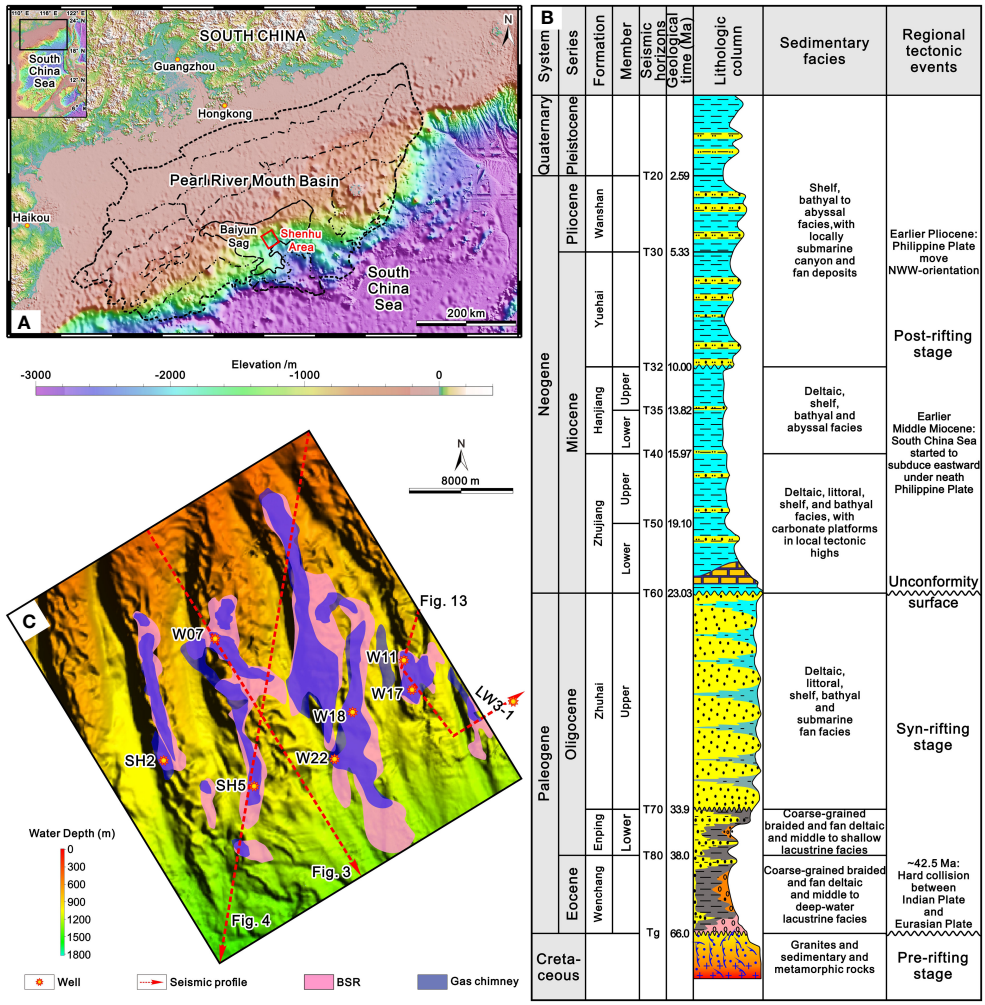

FIGURE 1
(A) Location of the Shenhu Area. **(B)** Multi-beam map of the seafloor and the locations of deep-water drillings in the study area (modified from Yang et al. (2015); Cheng et al. (2020); Zhang et al. (2020), and Zhu et al. (2021)). **(C)** Comprehensive stratigraphic column of the Pearl River Mouth Basin (modified from Shi et al. (2014); He et al. (2017), and Lei et al. (2021)).

curve and Vp curve values increase. At the same time, the DEN decreases, and the RES_BD_IMG highlight, showing a gas hydrate layer (Figure 2D). Additionally, beneath the hydrate layer, there exists a free gas layer where both the RES and Vp curve values experience a decline (Supplementary Data Sheet 1). The seismic profile displays a clear and prominent BSR characterized by high-amplitude reflections. Above the BSR, we can discern the gas hydrate layer, while below it lies the free gas layer. These layers exhibit significant and easily identifiable reflections on the seismic profiles (Figure 3). Faults and gas chimneys serve as favorable conduits for gas migration, facilitating the accumulation of gas hydrates and free gas beneath Well W07.

The values of the RES curve and Vp curve of Well W18 both dramatically rise at about 150 mbsf, while the value of the DEN curve falls (Figure 2E). The RES_BD_IMG distinctly highlights the presence of a gas hydrate layer, accompanied by a subsequent layer of free gas underneath. The gas hydrate layer exhibits an effective thickness of approximately 11.6 m, and the average saturation is approximately 30.5% (Supplementary Data Sheet 1).

Based on the analysis of well logging data, gas hydrates have been discovered at a depth of approximately 200 mbsf of Well SH2 (Figures 1C, 2F). The hydrate layer showcases a thickness of approximately 25 m and exhibits a saturation level of approximately 35.5% (Supplementary Data Sheet 1).

Well W11 is positioned north of Well W17 (Figures 1C, 2G). According to the RES curve, Vp curve, and RES_BD_IMG data, a thick gas hydrate layer can be identified, about 78.4 m, with an average saturation of about 22.9% (Supplementary Data Sheet 1). Furthermore, it is noteworthy that no occurrence of free gas has been observed beneath the gas hydrate layer (Figure 2G).

4.2 Gas migration pathways

4.2.1 Deep faults

The study area exhibits a widespread distribution of numerous deep faults that have developed over time (Figures 4, 5). Generally, the deep faults were active early, starting from the Eocene, and

10.3389/fmars.2023.1254410

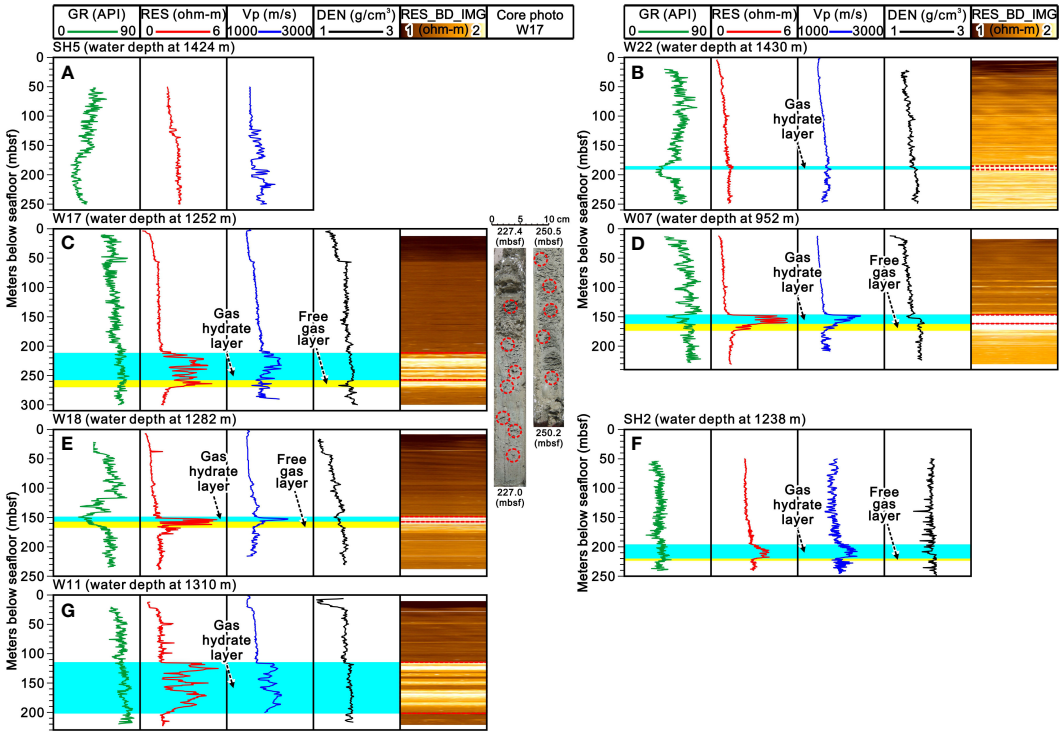

FIGURE 2
Gas hydrate occurrences in different wells. **(A)** Well logging data of Well SH5. **(B)** Well logging data and interpretations of Well W22. **(C)** Cores, well logging data, and interpretations of Well W17. **(D)** Well logging data and interpretations of Well W07. **(E)** Well logging data and interpretations of Well W18. **(F)** Well logging data and interpretations of Well SH2. **(G)** Well logging data and interpretations of Well W11.

lasted for a long time, and can be active until the Quaternary (Supplementary Data Sheet 2). In the study area, deep faults controlled sedimentary fillings according to the fault displacement. The persistent and long-term activities of faults can serve as pathways. Notably, numerous gas chimneys have developed in close proximity to these deep faults.

Multiple deep faults can be discerned on the coherence slice maps, primarily concentrated in the northern region of the study area (Figure 5). The orientation is NW and NWW, with a large extension length and a wide range of influence.

4.2.2 Branch faults

Branch faults are closely related to deep faults, generally developed after the formation of deep faults, with deep faults as the main faults and a series of faults formed in shallow strata (Figures 3, 4). Most branch faults have an opposite dip to the deep faults, but a few have the same. In the study area, the activity of branch faults has been observed to occur relatively late (Figure 4, Supplementary Data Sheet 2). It is notable that a significant number of branch faults have been activated after the late Miocene, resulting in their ability to cut through deep strata. However, according to the fault displacements, branch faults have little influence on sedimentary fillings. On the seismic profiles, branch and deep faults form flower-like structures (Figures 3, 4). The distribution of these faults can be visually observed on the coherence slice maps, displaying a distinctive broom- or horsetail-like shape in the overall planform (Figure 5). This pattern is indicative of the characteristics typically associated with strike-slip faults.

4.2.3 Gas chimneys

Many gas chimneys have developed within the study area, predominantly appearing as elongated columnar structures on the seismic profiles (Figures 3, 4). They are generally characterized by chaotic reflections at the bottom, acoustic blanking zone and pull-down anomalies on the body, and high-amplitude reflections at the top. Based on variations in their topographic shape, the gas chimneys within the study area can be categorized into different types, including mushroom-shaped, capsule-shaped, dome-shaped, and corolla-shaped gas chimneys. Among them, the mushroom-shaped gas chimney has been drilled to reveal the occurrence of gas hydrate and free gas (Figure 3). Furthermore, the gas chimneys can be further classified based on their root origin as either the Paleogene or the Neogene. Typically, their upper parts extend into the Quaternary layer and are linked to the BSR.

In the study area, the gas chimneys exhibit a long strip-like shape on the planform, primarily concentrated along the canyon ridges. Their predominant direction is mainly NNW (Figures 1C, 5). Also, their distribution is similar to the planform distribution of BSR, and their spatial distribution is well-matched, confirmed by the seismic profiles (Figures 3, 4).

TABLE 1 Gas geochemical data used in this study.

Well name	Water depth (m)	Sample depth	Sample type	$\delta^{13}C\text{-}C_1$ (‰)	$R=C_1/(C_2+C_3)$	$\delta^{2}H\text{-}C_1$ (‰)	Reference
LW3-1-1	1480	3070 m	Gas field gas	-37.1	12.2	-158.0	Liang et al. (2022)
		3189.5 m		-36.8	12.5	-156.0	
		3144.5 m		-36.6	12.5	-158.0	
		3499.5 m		-36.6	10.7	-176.0	
		3149–3154 m		-38.0	12	-151.0	
		3152.5 m		-37.9	12.4	-153.0	
		3175.5 m		-37.8	12.9	-142.0	
		3123.8 m		-37.5	13.1	-150.0	
		3123.5–3127.5 m		-37.3	13.2	-150.0	
		3123.5–3127.5 m		-37.4	13.2	-146.0	
W11	1310	101 mbsf	Hydrate gas	-65.0	3019	-170.4	Zhang et al. (2019)
		146 mbsf		-63.9	271	-180.7	
		153.5 mbsf		-65.0	285	-174.1	
		153.5 mbsf		-59.5	280	-178.0	
		171 mbsf		-64.9	239	-180.3	
		183 mbsf		-63.5	212	-175.3	
W17	1252	51.6 mbsf	Hydrate gas	-73.8	619	-144.1	Zhang et al. (2019)
		87.5 mbsf		-63.7	595	-142.0	
		222 mbsf		-55.7	171	-149.5	
		241 mbsf		-60.9	222	-180.5	
		263 mbsf		-62.4	236	-179.9	
W18	1282	146 mbsf	Hydrate gas	-38.4	1561	-154.0	Zhang et al. (2019)
		149 mbsf		-38.4	1318	-137.7	
		159.5 mbsf		-34.9	643	-156.6	
		171.5 mbsf		-41.1	162	-130.0	
SC-1	/	155.35–155.48 mbsf	Hydrate gas	-49.5	426	-165	Lai et al. (2022)
		160.02–160.13 mbsf		-48.9	156	-180	
		160.58–160.76 mbsf		-49.1	183	-163	
		161.43–161.63 mbsf		-49.5	72	-175	
		163.25–163.46 mbsf		-50.2	115	-169	
SC-2	/	158.68–158.84 mbsf	Hydrate gas	-47.4	142	-173	Lai et al. (2022)
		169.85–170.08 mbsf		-47.5	71	-179	
SC-W01B	/	135.7 mbsf	Hydrate gas	-50	1338.3	-170.3	Liang et al. (2022)
		155.48 mbsf		-47	302.4	-190.7	

(Continued)

10.3389/fmars.2023.1254410

TABLE 1 Continued

Well name	Water depth (m)	Sample depth	Sample type	$\delta^{13}C$-C_1 (‰)	$R=C_1/(C_2+C_3)$	$\delta^{2}H$-C_1 (‰)	Reference
		160.13 mbsf		-47.1	121.4	-195.1	
		160.76 mbsf		-49.2	119.6	-195	
SC-W01C	/	147.35 mbsf	Hydrate gas	-48.2	755.3	-183.5	Liang et al. (2022)
		148.21 mbsf		-47.4	1792.5	-186.3	
		161.63 mbsf		-47.8	56.9	-196.6	
		162.16 mbsf		-47.6	79.9	-191.2	
		163.46 mbsf		-48.1	75.4	-191.9	
SC-W02B	/	143.54 mbsf	Hydrate gas	-46.7	437.3	-185.8	Liang et al. (2022)
		144.52 mbsf		-46.2	276.2	-191.9	
		158.84 mbsf		-47.3	60.1	-197.9	
		170.08 mbsf		-46.9	57.8	-193.5	
SC-W03B	/	136.57 mbsf	Hydrate gas	-65.2	316.7	-191.3	Liang et al. (2022)
		/		-66.2	342.4	-192.6	
		/		-66.6	462.4	-194	
		/		-66.6	464.4	-193.1	
SC-2017	/	/	Hydrate gas	-64.9	198.3	-191.6	Liang et al. (2022)
		/		-63.9	199.4	-191.8	
		/		-64.9	204	-188.7	
		/		-64.8	200.9	-190.7	
		/		-65	203.1	-188.8	
		/		-65.1	202.1	-190.4	
		/		-65	193.4	-190.3	
		/		-64.9	202.4	-192.8	
		/		-64.9	201.6	-194	
		/		-65.1	203.3	-192.4	
		/		-65.1	198.4	-189	
		/		-64.8	213.9	-191	
		/		-64.6	214.2	-190.4	
		/		-64.5	218.6	-191.6	
		/		-65	210.2	-186	
		/		-65.2	209.8	-192.4	
		/		-65.2	206.3	-192.8	
		/		-65	205.9	-188.5	
		/		-65.2	215.7	-191.4	
		/		-65.3	215.9	-187.6	
		/		-65.1	210.1	-190.8	
		/		-65.1	211.4	-194.3	
		/		-65	213.3	-195.4	

(Continued)

10.3389/fmars.2023.1254410

TABLE 1 Continued

Well name	Water depth (m)	Sample depth	Sample type	$\delta^{13}C$-C_1 (‰)	$R=C_1/(C_2+C_3)$	$\delta^{2}H$-C_1 (‰)	Reference
		/		-65	215.7	-193.9	
		/		-64.9	214.2	-195.3	
		/		-64.7	206.9	-192.4	
		/		-64.8	209.3	-192.6	
		/		-65	210.1	-190.4	
		/		-65	213.7	-190.5	
		/		-64.8	207.9	-190.7	
		/		-64.8	211.6	-192	
		/		-65	208.4	-191.6	
		/		-64.7	214.7	-189.7	
		/		-65.3	199.6	-187.8	
		/		-64.8	200.5	-193.9	
		/		-65.3	197.3	-191	
		/		-65.1	193	-194.2	
		/		-65.3	197.7	-188.1	
		/		-65.2	198.3	-189	
		/		-65.1	203.7	-194	
		/		-65.2	195.5	-193.5	
		/		-65.2	195.4	-195.7	
		/		-65.1	199.7	-188.5	
SC-2020	/	/	Hydrate gas	-65.2	182.3	-184.6	Liang et al. (2022)
		/		-64.9	177.9	-188.3	
		/		-64.5	189.9	-188.8	
		/		-64.5	184.2	-188.5	
		/		-64.4	179.8	-190.3	
		/		-64	159.8	-191.2	
		/		-64.5	177.8	-185.7	
		/		-64.7	184.7	-187.7	
		/		-64.3	201.3	-186.5	
		/		-64.3	182.4	-186.9	
		/		-64.6	183.5	-190.4	
		/		-64.4	182.2	-186.4	
		/		-64.7	216.1	-185.5	
		/		-64.5	232.2	-187.9	
		/		-64.4	210	-185	
		/		-64.8	232	-177.4	
		/		-64.4	241	-185	
		/		-64.4	216.4	-189.3	
		/		-64.3	227.3	-189.4	

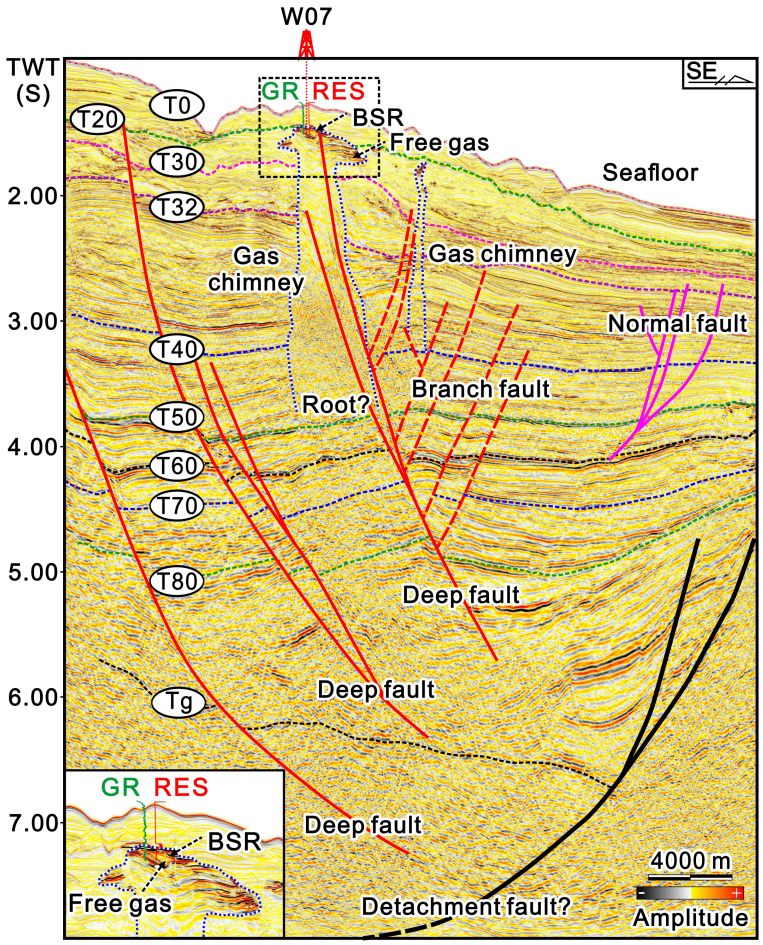

FIGURE 3
Interpreted seismic profile crossed Well W07 shows the typical characteristics of BSR.

4.3 Coupled model of faults and gas chimneys

In this study, according to the coupling relationship of deep faults, branch faults, and gas chimneys under drilling constraints, seven different geological models can be identified (Figures 3, 6, 7, 8). The geological models can be categorized into two groups: gas chimney-based and fault-based, with the gas chimney serving as a supplementary factor. Within the gas chimney-based models, there are two subdivisions: Model-SH5 and Model-W22, based on the origins of the gas chimneys. On the other hand, the fault-dominated geological model, supplemented by gas chimneys, can be further divided into Model-W17, Model-W07, Model-W18, Model-SH2, and Model-W11, based on the type and timing of deep faults, branch faults, and the origins of gas chimneys.

4.3.1 Model-SH5

Model-SH5, a gas chimney-based structure, traces its origin to the Zhujiang Formation and terminates in the Quaternary layer. It is characterized by a dome-shaped top, as illustrated in Figure 6A. Micro-fractures are observed within the gas chimney, leading to chaotic reflections. The seismic profile reveals pull-down anomalies along the body, high-amplitude reflections at the top, and the presence of the BSR. It is worth noting that no gas hydrate was encountered during drilling, as depicted in Figure 2A.

4.3.2 Model-W22

The Model-W22 is also gas chimney-based, which originated in the Wenchang-Enping Formations and terminated in the Quaternary, with a mushroom-shaped top (Figure 6B). The lower part of the gas chimney mainly shows chaotic reflections and no apparent micro-fractures are seen; the upper part has pull-down anomalies, and the top shows high-amplitude reflections. Based on the drilling results from Well W22, a thin layer of gas hydrate is observed atop the gas chimney (Figure 2B).

4.3.3 Model-W17

The Model-W17 is dominated by a deep fault, which has been active since the Eocene, liking source rocks and shallow formations (Figure 7A). The gas chimney is developed on the deep fault, originating in the Wenchang-Enping Formations and terminating in the Quaternary, and have a mushroom-shaped top. The interior of the gas chimney exhibits pull-down anomalies, while the upper portion reveals an acoustic blanking zone. The top of the gas

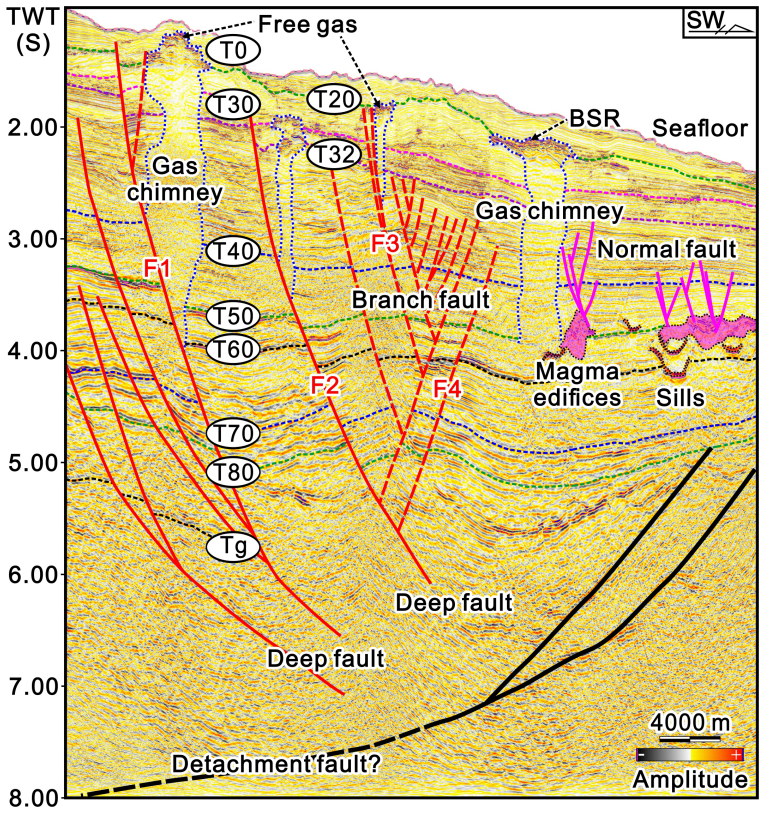

FIGURE 4
Interpreted typical seismic profile in the study area shows deep faults, branch faults, and gas chimneys.

chimney displays high-amplitude reflections resulting from the accumulation of free gas. Concurrently, drilling activities have confirmed the presence of gas hydrates and free gas in the area (Figure 2C).

4.3.4 Model-W07

Similar to Model-W17, Model-W07 is also dominated by deep faults (Figure 3). The deep faults were active early and continued until the Quaternary. The difference is that the gas chimney of Model-W07 originates from the Zhujiang Formation and terminates in the Quaternary. The lower part of the gas chimney shows chaotic reflections, the body is an acoustic blanking zone, and the top is high-amplitude reflections, mushroom-shaped. Moreover, the presence of gas hydrates and free gas has been confirmed based on the findings from Well W07 (Figure 2D).

4.3.5 Model-W18

Model-W18 is also deep fault-dominated, and branch fault plays an important role in gas migration (Figure 7B). Deep fault has been active since the Eocene, connecting deep and shallow strata and even the seafloor. The branch fault was active later but also cut the Wenchang Formation. The gas chimney is developed on a branch fault, originating from the Wenchang-Enping Formations and terminating in the Quaternary, with a mushroom-shaped top. A chaotic reflection zone, an acoustic blanking zone, and pull-down anomalies primarily characterize bottom-up features. A high-amplitude zone is also formed at the top due to gas hydrates and free gas (Figure 2E).

4.3.6 Model-SH2

Model-SH2 is similar to Model-W18, mainly controlled by deep faults and branch faults, all of which are connected with source rocks (Figure 8A). The difference is that the gas chimney of Model-SH2 originates from the Lower Miocene Zhujiang Formation, connects with branch fault at the bottom, terminates at the Pliocene Wanshan Formation, and has a corolla-shaped top. Minor faults are observed at the upper section of the gas chimney, connecting it to the BSR. These faults serve as conduits for transporting free gas to the GHSZ, contributing to forming gas hydrates (Figure 2F).

4.3.7 Model-W11

Model-W11 is dominated by a deep fault, branch fault, and gas chimney (Figure 8B). The deep fault has been active for a long time, connecting the source rocks. The activity of branch faults was initiated relatively late, specifically during the Middle and Late Miocene period. The gas chimney is developed on a branch fault, originating from the Hanjiang Formation and terminating in the Quaternary, and the top is still mushroom-shaped. The internal events of the gas chimney are relatively continuous, with pull-down anomalies. The presence of a distinct BSR is evident at the top, indicating the occurrence of thick gas hydrate deposits (Figure 2G).

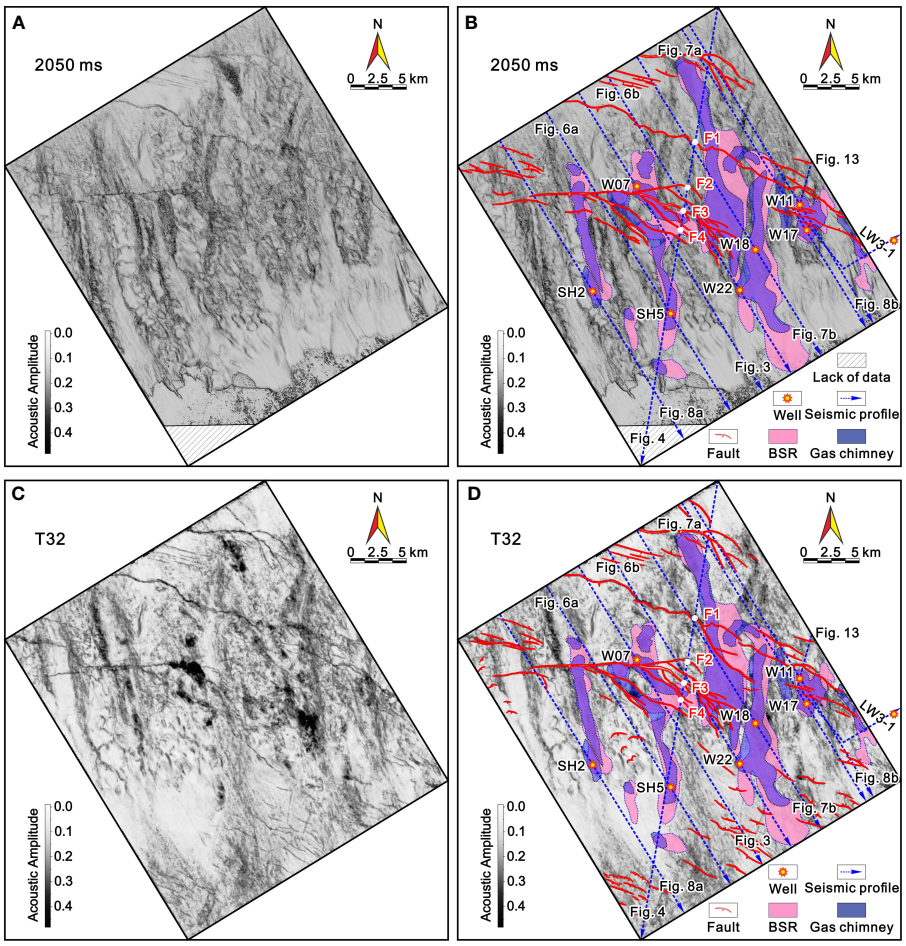

FIGURE 5
(A) Uninterpreted and **(B)** interpreted coherence slice map of 2050 ms. **(C)** Uninterpreted and **(D)** interpreted coherence slice map of Horizon T32. White circles are selected points of faults for calculating fault activities.

5 Discussion

5.1 Gas origin of hydrates in the Shenhu Area

Recent studies have highlighted the increasing significance of gas geochemical data analysis for identifying the origin of gas derived from hydrates. This emerging area of research has garnered considerable attention within the field of gas hydrate exploration (Sassen et al., 2001; Milkov, 2005; Feng et al., 2009; Wu et al., 2011; Portnov et al., 2021; Wei et al., 2021; Lai et al., 2023). Milkov and Etiope (2018) have introduced genetic diagrams that have gained global popularity, encompassing various plots. This study mainly analyzed three types of gas geochemical data collected from four wells (Table 1) (Zhang et al., 2019; Lai et al., 2022; Liang et al., 2022).

One hundred eleven gas samples used in this study are plotted in the genetic diagrams (Figure 9) so as to determine the source of hydrate gas. Five samples from Well W17 are plotted in the genetic diagrams, which mainly show the characteristics of microbial-thermogenic mixing origin (Figure 9) (Bernard et al., 1977). There are not only contributions from *in situ* microbial gas but also contributions from deep thermogenic gas. In addition, one data point may be related to the secondary microbial gas, just like samples from Wells SC-1 and SC-2, indicating that the deep thermogenic gas was modified by microorganisms during the upward migration to the shallow strata (Figure 9A) (Lai et al., 2022). Four samples taken from Well W18 are primarily situated within the thermogenic gas field. Among these, three samples indicate late mature thermogenic gas, and one may be attributed to secondary microbial gas (Figure 9). The analysis reveals a strong correlation between the gas extracted from hydrates in Well W18 and deep thermogenic gas. This correlation is notably linked to the Paleogene source rocks present in the study area (Figure 7B). Six data points obtained from Well W11 have been plotted, indicating that the majority of these data points are attributed to microbial-thermogenic mixing origin. Similar results to those of Well W17 may be due to the close distance between the two drillings (Figures 1C, 9). It is essential to acknowledge that the gas hydrates in Well W11 also derive contributions from deep thermogenic gas sources. In situ, microbial gas in both Well W11 and Well W17 is also attributed to CO_2 reduction processes

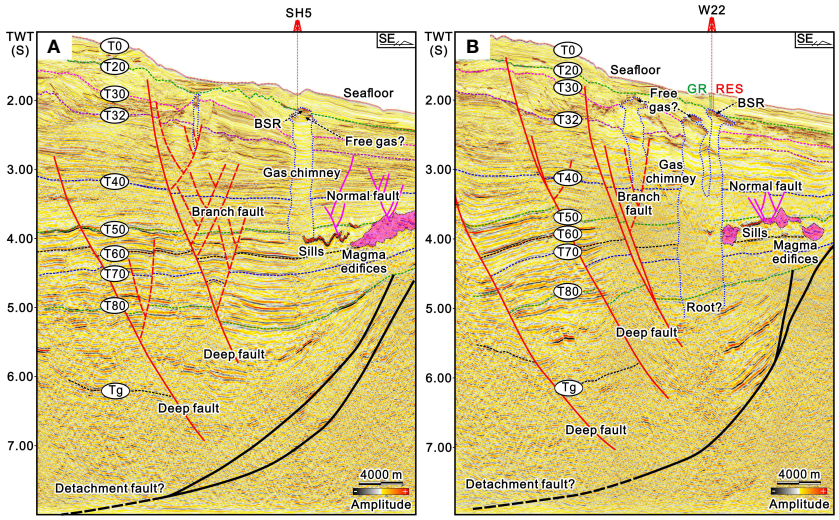

FIGURE 6
(A) Interpreted seismic profile crossed Well SH5. **(B)** Interpreted seismic profile crossed Well W22.

(Bernard et al., 1977; Whiticar et al., 1986; Whiticar, 1999; Zhang et al., 2019; Lai et al., 2022; Liang et al., 2022).

Ten samples obtained from the LW3-1 gas field exhibit distinct characteristics compared to samples collected from the other three wells. These specific samples originate from the deep natural gas reservoirs found within the Zhuhai Formation and Zhujiang Formation of the LW3-1 gas field (Figure 1C, Table 1). Based on the genetic diagrams, the analyzed samples primarily consist of thermogenic gas, particularly oil-associated thermogenic gas. The data points presented in Figure 9 provide substantial support for this conclusion. It is worth noting that the LW3-1 gas field has undergone several years of product development. Extensive research has been conducted in previous studies to investigate the gas source of the area, leading to the belief that the primary natural gas supply originates from lacustrine source rocks within the Wenchang Formation and Enping Formation (Dai et al., 2017; Zhu et al., 2021).

According to previous studies, a large number of data from other drillings in the Shenhu Area, including SC-W01B, SC-W01C, SC-W02B, SC-W03B, SC-2017, and SC-2020, show that hydrate gas is of mixed origin. In addition to biogenic gas, it confirms the contribution of thermogenic gas (Liang et al., 2022). Figure 1C clearly illustrates the proximity of the LW3-1 gas field to the study area, indicating its close proximity to the W17, W18, and W11 drill sites. The gas samples from these four wells all have traces of thermogenic gas. By considering the gas source of the LW3-1 gas

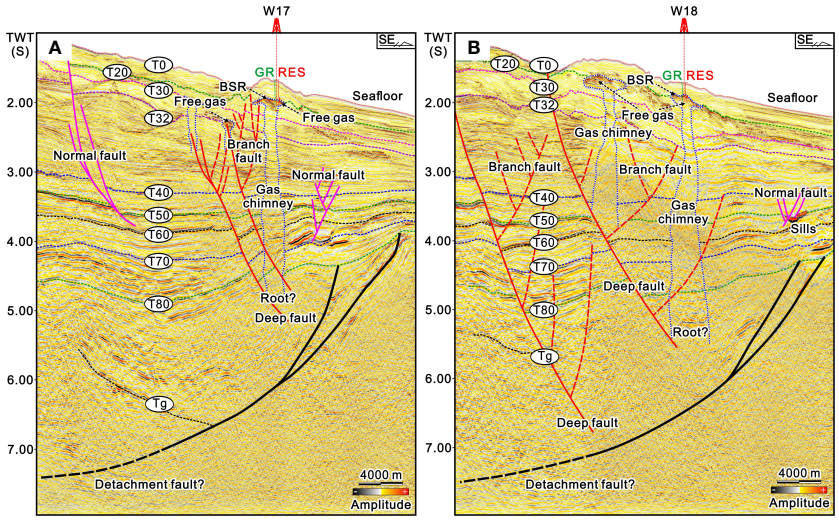

FIGURE 7
(A) Interpreted seismic profile crossed Well W17. **(B)** Interpreted seismic profile crossed Well W18.

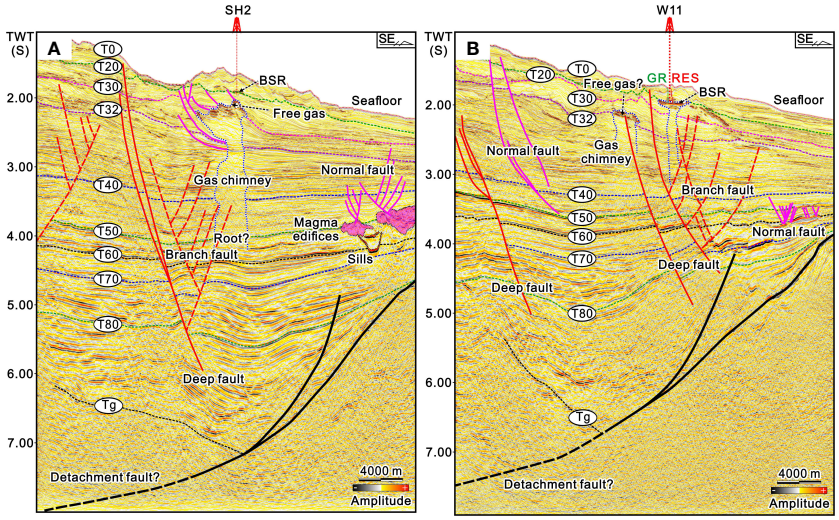

FIGURE 8
(A) Interpreted seismic profile crossed Well SH2. **(B)** Interpreted seismic profile crossed Well W11.

field, it can be inferred that the gas within the hydrates may have originated from the thermogenic gas present in the Wenchang, Enping, and Zhuhai Formations (Mi et al., 2018; Pang et al., 2018).

5.2 Contribution of different coupled geological models to gas hydrate accumulation

This study utilizes core-log-seismic data from the study area to establish seven integrated geological models of faults and gas chimneys (Figure 10). Subsequently, statistical analyses are conducted to examine the occurrences of gas hydrates and free gas as revealed by the drillings conducted within each model (Figure 11, Supplementary Data Sheet 1). Among them, the gas chimneys in Model-SH5 and Model-W22 both serve as the main gas migration pathways and contribute little to gas hydrate accumulation (Figures 10A, B, 11). Model-SH5 did not yield any gas hydrate discoveries, while Model-W22 exhibited only a thin layer of hydrates with a saturation of less than 10%. This observation may be attributed to the fact that the gas chimney in Model-W22 originated from a thermogenic gas zone (Cheng et al., 2020; Wan et al., 2022).

Deep faults and gas chimneys act as the main gas migration pathways in Model-W17 and Model-W07 (Figures 10C, D). The difference is that the former gas chimney originates from the deep thermogenic gas zone, while the latter originates from the shallow microbial gas zone. Based on the drilling results depicted in Figure 2, both Model-W17 and Model-W07 exhibit the presence of gas hydrates and free gas. Notably, Model-W17 shows a more significant contribution to hydrate accumulation compared to Model-W07. Moreover, illustrated in Figure 9, the geochemical analysis unveils that the gas confined within hydrates of Model-W17 emanates from thermogenic origins. This substantiates the

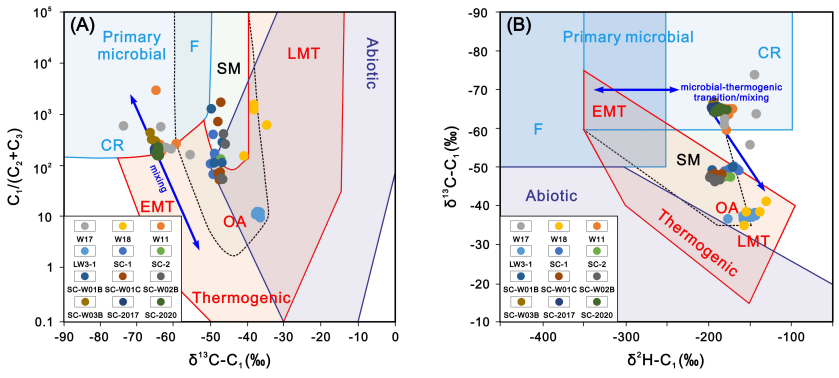

FIGURE 9
(A) Genetic diagram of $R=C_1/(C_2+C_3)$ versus $\delta^{13}C\text{-}C_1$. **(B)** Genetic diagram of $\delta^{13}C\text{-}C_1$ versus $\delta^{2}H\text{-}C_1$. These diagrams are modified from Milkov and Etiope (2018) and Snodgrass and Milkov (2020). The gas geochemical data are obtained from Zhang et al. (2019), Lai et al. (2022), and Liang et al. (2022). CR-CO_2 reduction, EMT-early mature thermogenic gas, F-methyl-type fermentation, LMT-late mature thermogenic gas, OA-oil-associated thermogenic gas, SM-secondary microbial.

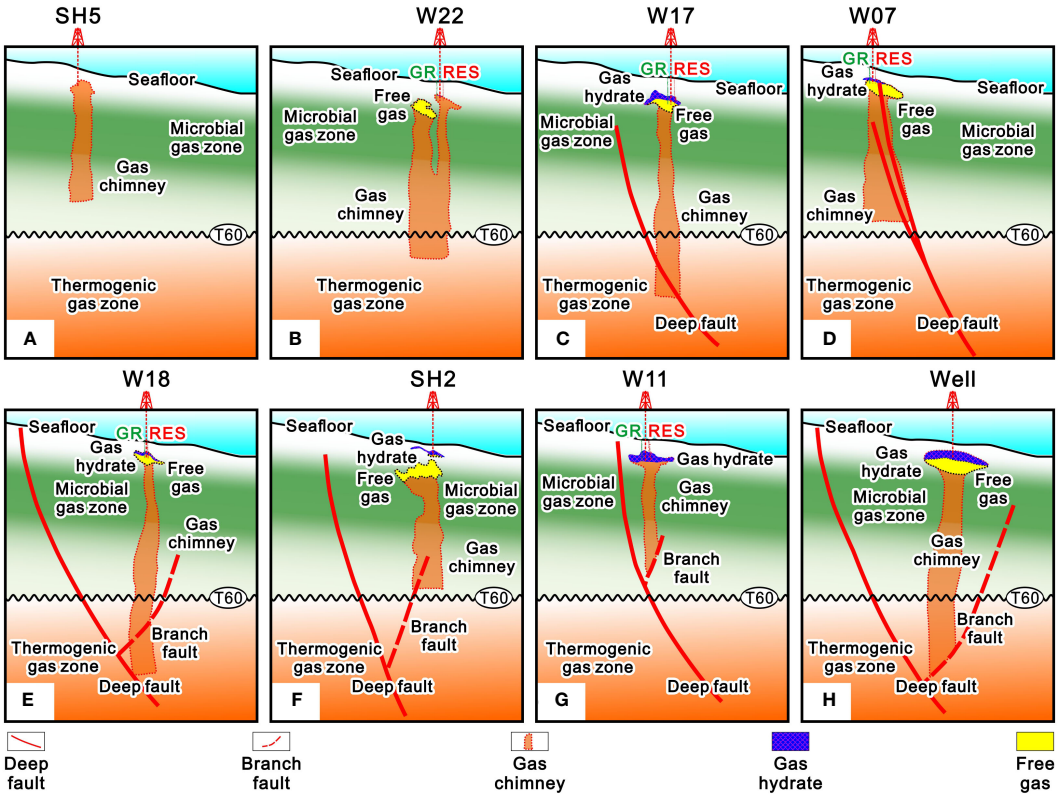

FIGURE 10
Simplified schematic diagrams of the coupled geological models of faults and gas chimneys (not to scale). **(A)** Gas chimney-based Model-SH5, and the gas chimneys originate from the microbial gas zone. **(B)** Gas chimney-based Model-W22, and the gas chimneys originate from the thermogenic gas zone. **(C)** Fault-based and gas chimney supplemented Model-W17, and the gas chimneys originate from the thermogenic gas zone. **(D)** Fault-based and gas chimney supplemented Model-W07, and the gas chimneys originate from the microbial gas zone. **(E)** Fault-based and gas chimney supplemented Model-W18, the branch fault is connected to the Paleogene, and the gas chimney originates from the thermogenic gas zone. **(F)** Fault-based and gas chimney supplemented Model-SH2, the branch fault is connected to the Paleogene, and the gas chimney originates from the microbial gas zone. **(G)** Fault-based and gas chimney supplemented Model-W11, the branch fault is connected to the Neogene, and the gas chimney originates from the microbial gas zone. **(H)** A summarized geological model conducive to gas hydrate accumulation mainly consists of deep fault, branch fault, and gas chimney originating from the thermogenic gas zone.

presence of vertical migration pathways, such as deep faults and gas chimneys, affirming their role in facilitating gas migration. These findings underscore the pivotal role these pathways play in facilitating the accumulation of gas hydrates (Zhang et al., 2019).

The gas migration pathways of Model-W18, Model-SH2, and Model-W11 are all composed of deep faults, branch faults, and gas chimneys (Figures 10E–G). The branch fault of Model-W18 cut to the deep strata, and the gas chimney also originates from the thermogenic gas zone located on the branch fault (Figure 10E). In contrast, the gas chimney originates in the microbial gas zone in Model-SH2 (Figure 10F). The branch fault observed in Model-W11 exhibited late activity and did not penetrate the deep thermogenic gas zone (Figure 10G). The gas chimneys in these two models are rooted in the Neogene and are situated along branch faults. The drilling results indicate favorable gas hydrates and free gas occurrences in each model. Additionally, the gas geochemical data from Model-W18 and Model-W11 further support the presence of thermogenic gas (Figures 9, 11). However, it is noteworthy that in Model-W18, both the branch fault and the bottom root of the gas chimney are situated within the thermogenic gas zone. As a result, the gas samples exhibit distinct characteristics indicative of late-stage maturation of thermogenic gas.

Evident from the analysis of the seven geological models, it becomes apparent that the influence of gas chimney-based geological models on gas hydrate accumulation is notably overshadowed by the prominence of deep fault-based geological models supplemented by gas chimneys and branch faults (Figure 10). The absence of free gas layer in Model-W22 may be because this model has no deep faults. Deep thermogenic gas cannot migrate and accumulate in considerable quantities vertically. The reason for Model -W11 may be similar; the gas chimney is not directly connected to the fault active in the deep source rock. Moreover, we overlayed the planform distribution of faults and gas chimneys onto the coherence slice map of Horizon T32. The observation reveals that in areas where both faults and gas chimneys are present, the occurrence of gas hydrates and free gas is notably more substantial compared to regions where only gas chimneys are developed. This finding further emphasizes the influential role of fault systems in governing the accumulation of gas hydrates (Figure 12) (Jin et al., 2020; Sun et al., 2020; Zhang et al., 2023). Hence, the integrated geological models incorporating

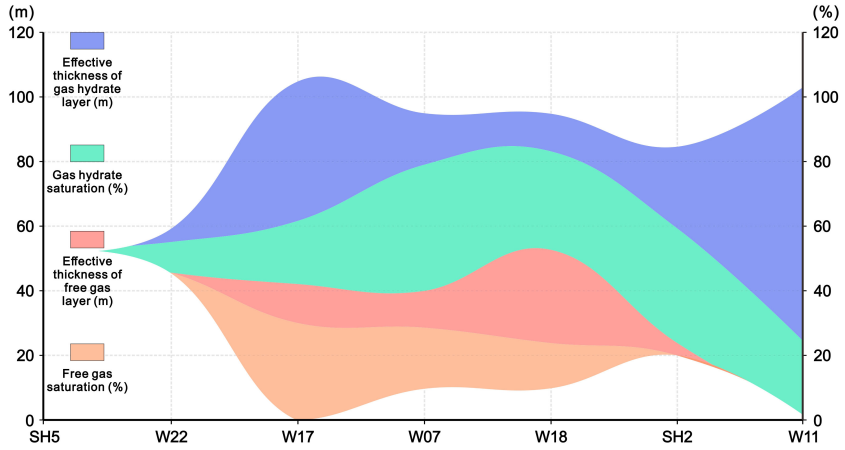

FIGURE 11
Stream Chart shows the occurrence of gas hydrate and free gas under different drilling constraints.

deep faults, gas chimneys, and branch faults hold great significance in understanding the processes involved in gas hydrate accumulation (Figure 10H).

5.3 Implications for gas hydrate exploration and industrialization

By analyzing gas geochemical data and assessing the contribution of various geological models that encompass faults and gas chimneys to the accumulation of gas hydrates, the significant influence of deep faults in gas hydrate systems becomes evident. Similarly, it is evident that the primary gas migration pathways, including the LW3-1 gas field, are predominantly associated with deep faults (Wu et al., 2018; Jin et al., 2020). Consequently, we chose a seismic profile that intersects the gas hydrate wells and the LW3-1 gas field to examine the interrelationship between deep natural gas reservoirs, shallow free gas/shallow gas reservoirs, and gas hydrates (Figure 13).

The thermogenic gas, derived from source rocks such as the Wenchang Formation and Enping Formation, exhibits vertical migration along deep faults towards the Zhuhai Formation and Zhujiang Formation, resulting in the formation of deep natural gas reservoirs. The gas geochemical data further validate that the gas present in the LW3-1 gas field is primarily oil-associated thermogenic gas (Figure 9) (Zhu et al., 2009). With the accumulation of gas, the

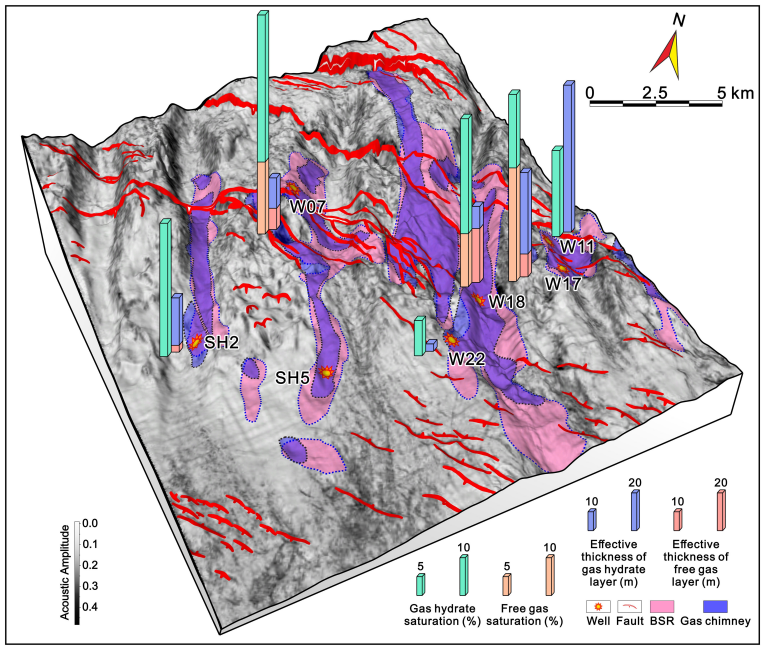

FIGURE 12
Coherence slice map of Horizon T32 superimposed gas hydrate and free gas occurrences, faults, gas chimneys, and BSRs.

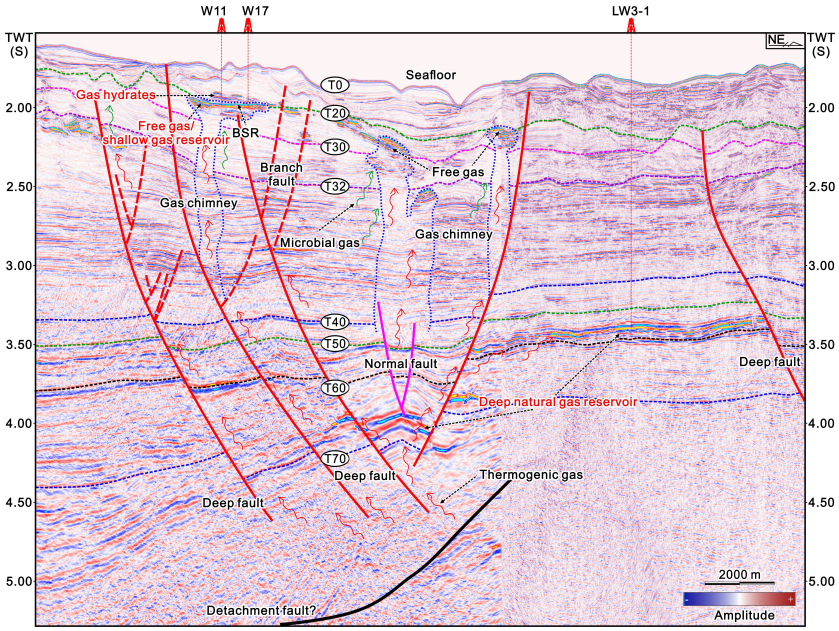

FIGURE 13
Typical seismic profile crossed gas hydrate drillings Well W11, Well W17, and LW3-1 gas field. Deep thermogenic gas can migrate along faults to accumulate in the Zhujiang Formation, forming deep natural gas reservoirs (LW3-1 gas field). They have the potential to migrate vertically towards the shallow strata through faults and gas chimneys. This process can lead to the accumulation of gas together with secondary microbial gas and *in situ* microbial gas, resulting in the formation of shallow gas reservoirs. Gas can then migrate vertically toward the gas hydrate stability zone, ultimately forming gas hydrates.

formation fluid pressure in deep natural gas reservoirs increases, resulting in overpressures. It is generally believed that the Dongsha movement is the trigger for the release of overpressures, which will lead to the migration of fluids (Guo et al., 2016; Kong et al., 2018). The Baiyun sag has been scientifically confirmed to possess a record of intermittent occurrences of overpressure events. These events have served as the driving mechanism for the vertical migration of deep thermogenic gas towards the shallow strata through faults and gas chimneys (Figure 13). Moreover, the formation of shallow gas reservoirs ensures a continuous and high-flux supply of gas, contributing to the accumulation of gas hydrates within the upper GHSZ. Ultimately, this comprehensive interplay forms a complete gas hydrate system (Figure 13).

Thermogenic gas plays a crucial role as a significant gas source for multiple components, including the deep natural gas reservoirs within the LW3-1 gas field, as well as the shallow gas reservoirs and

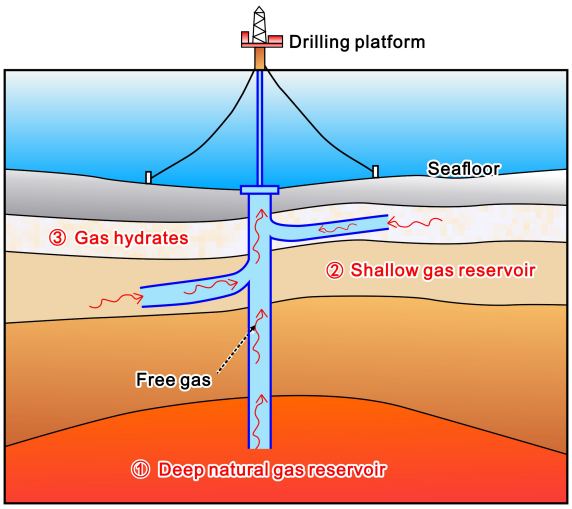

FIGURE 14
Three-gas combined production model for exploring and developing deep natural gas reservoirs, shallow gas reservoirs, and gas hydrates as a whole system (not to scale).

gas hydrates within Wells W11 and W17 in the study area. It is also important to acknowledge the contributions of shallow *in situ* microbial gas and secondary microbial gas in this context (Figure 9). Hence, it can be deemed feasible to explore and develop deep natural gas reservoirs, shallow gas reservoirs, and gas hydrates as a complete system in a marine environment (Figure 14). The implementation of a three-gas combined production model holds the potential to enhance the optimization of design for deep-water drilling and production projects. This model enables efficient development of deep-water natural gas resources and represents a cutting-edge direction for the future of oil and gas fields. Embracing such an approach is of immense significance in ensuring national energy development. Even so, there still exist several technical challenges that necessitate the collaboration of multidisciplinary scientists to address this juncture (Bai and Zhou, 2022).

6 Conclusions

By leveraging the most recent core-log-seismic data, this paper provides comprehensive documentation of the occurrence of gas hydrates, the diverse types of gas migration pathways, and the distinct characteristics of geological models integrating faults and gas chimneys. In conjunction with gas geochemical data, an analysis of the gas origin within hydrates and the contribution of each geological model to gas hydrate accumulation is presented. Based on these findings, a three-gas combined production model is proposed, offering valuable insights for future research and development in the field. The detailed conclusions are as follows:

1. The gas origin of hydrates mainly includes three types: thermogenic gas produced by the Paleogene source rocks, secondary microbial gas formed from thermogenic gas transformed by microorganisms, and shallow *in situ* microbial gas. Significantly, deep thermogenic gas has been established as a vital gas source for gas hydrate formation, a finding substantiated by drilling activities. Gas samples from hydrates in Well W18 show obvious characteristics of late mature thermogenic gas.
2. The study area reveals three primary types of gas migration pathways: deep faults, branch faults, and gas chimneys. Among these, deep faults assume a pivotal role in enabling the vertical migration of thermogenic gas.
3. According to the types of gas migration pathways, seven different coupled models of faults and gas chimneys can be established. Through an integration of the drilling results, it becomes evident that the geological model incorporating deep faults and gas chimneys plays a crucial role in facilitating the accumulation of gas hydrates. These geological features effectively control the occurrence of gas hydrates and free gas.
4. The implementation of a three-gas combined production model, incorporating deep natural gas reservoirs, shallow gas reservoirs, and gas hydrates, represents an auspicious approach for future endeavors in deep-water oil and gas exploration and production. This integrated model holds substantial potential in optimizing resource utilization and maximizing operational efficiency in these domains. However, its successful implementation necessitates extensive interdisciplinary collaboration among scientists.

Data availability statement

The original contributions presented in the study are included in the article/Supplementary Material. Further inquiries can be directed to the corresponding authors.

Author contributions

JR: Formal Analysis, Investigation, Resources, Writing – original draft. CC: Conceptualization, Formal Analysis, Investigation, Methodology, Writing – original draft, Writing – review & editing. TJ: Formal Analysis, Funding acquisition, Investigation, Project administration, Supervision, Writing – review & editing. ZK: Investigation, Resources, Supervision, Writing – review & editing, Funding acquisition. HL: Formal Analysis, Investigation, Resources, Writing – review & editing. JL: Formal Analysis, Funding acquisition, Resources, Writing – review & editing. ZC: Formal Analysis, Investigation, Writing – review & editing. TL: Formal Analysis, Investigation, Writing – review & editing.

Funding

Financial support for this research was provided by the National Natural Science Foundation of China under Grants 42376221, 41976073, and 42276073, the Guangdong Major Project of Basic and Applied Basic Research under Grant 2020B0301030003, the Director Research Fund Project of Guangzhou Marine Geological Survey under Grant 2023GMGSJZJJ00030, and the China Geological Survey Project under Grant DD20230064.

Acknowledgments

We want to extend our heartfelt gratitude to the Guangzhou Marine Geological Survey for allowing us to share our research findings through this publication. Furthermore, we wish to express our sincere appreciation to the esteemed editorial team, Guest Associate Editor Dr. Fei Han, and the reviewers for their valuable insights, suggestions, and constructive feedback, which have greatly contributed to the enhancement of this work.

Conflict of interest

The authors declare that the research was conducted in the absence of any commercial or financial relationships that could be construed as a potential conflict of interest.

The reviewer SY declared a shared affiliation with the authors JR, ZK, HL, and JL to the handling editor at the time of review.

Publisher's note

All claims expressed in this article are solely those of the authors and do not necessarily represent those of their affiliated organizations, or those of the publisher, the editors and the reviewers. Any product that may be evaluated in this article, or claim that may be made by its manufacturer, is not guaranteed or endorsed by the publisher.

Supplementary material

The Supplementary Material for this article can be found online at: https://www.frontiersin.org/articles/10.3389/fmars.2023.1254410/full#supplementary-material

References

Bai, R., and Zhou, S. (2022). China's deepwater gas hydrate development strategies under the goal of carbon peak. *Natural Gas Industry* 42, 156–165.

Beaudoin, Y., Waite, W., Boswell, R., and Dallimore, S. (2014). *Frozen heat: A UNEP global outlook on methane gas hydrates. Volume 1* (Kirkland Trykkery A/S, Norway: United Nations Environment Programme).

Bernard, B., Brooks, J. M., and Sackett, W. M. (1977). "A Geochemical Model for Characterization of Hydrocarbon Gas Sources," in *Marine Sediments, Offshore Technology Conference*. (Houston, Texas: OnePetro). OTC–2934-MS.

Boswell, R., and Collett, T. S. (2011). Current perspectives on gas hydrate resources. *Energy Environ. Sci.* 4, 1206–1215. doi: 10.1039/C0EE00203H

Chen, D., Wu, S., Dong, D., Mi, L., Fu, S., and Shi, H. (2013). Focused fluid flow in the Baiyun Sag, northern South China Sea: implications for the source of gas in hydrate reservoirs. *Chin. J. Oceanol Limnol* 31, 178–189. doi: 10.1007/s00343-013-2075-5

Cheng, C., Jiang, T., Kuang, Z., Yang, C., Zhang, C., He, Y., et al. (2020). Characteristics of gas chimneys and their implications on gas hydrate accumulation in the Shenhu area, northern South China Sea. *J. Natural Gas Sci. Eng.* 84, 103629. doi: 10.1016/j.jngse.2020.103629

Chong, Z. R., Yang, S. H. B., Babu, P., Linga, P., and Li, X.-S. (2016). Review of natural gas hydrates as an energy resource: Prospects and challenges. *Appl. Energy* 162, 1633–1652. doi: 10.1016/j.apenergy.2014.12.061

Collett, T. S., Boswell, R., Waite, W. F., Kumar, P., Roy, S. K., Chopra, K., et al. (2019). India National Gas Hydrate Program Expedition 02 Summary of Scientific Results: Gas hydrate systems along the eastern continental margin of India. *Mar. Petroleum Geology* 108, 39–142. doi: 10.1016/j.marpetgeo.2019.05.023

Collett, T. S., Johnson, A., Knapp, C. C., and Boswell, R. (2009). "Natural gas hydrates: A review," in *Natural gas hydrates—Energy resource potential and associated geologic hazards: AAPG Memoir*, (Tulsa, OK, United States: The American Association of Petrole), vol. 89 . Eds. T. Collett, A. Johnson, C. Knapp and R. Boswell, 146–219.

Cook, A. E., Portnov, A., Heber, R. C., Vadakkepuliyambatta, S., and Bünz, S. (2023). Widespread subseafloor gas hydrate in the Barents Sea and Norwegian Margin. *Earth Planetary Sci. Lett.* 604, 117993. doi: 10.1016/j.epsl.2023.117993

Dai, J., Ni, Y., Huang, S., Peng, W., Han, W., Gong, D., et al. (2017). Genetic types of gas hydrates in China. *Petroleum Explor. Dev.* 44, 887–898. doi: 10.1016/S1876-3804(17)30101-5

Davies, R. J., Yang, J., Hobbs, R., and Li, A. (2014). Probable patterns of gas flow and hydrate accretion at the base of the hydrate stability zone. *Geology* 42, 1055–1058. doi: 10.1130/G36047.1

Dickens, G. R., O'Neil, J. R., Rea, D. K., and Owen, R. M. (1995). Dissociation of oceanic methane hydrate as a cause of the carbon isotope excursion at the end of the Paleocene. *Paleoceanography* 10, 965–971. doi: 10.1029/95PA02087

Feng, D., Chen, D., and Roberts, H. H. (2009). Petrographic and geochemical characterization of seep carbonate from Bush Hill (GC 185) gas vent and hydrate site of the Gulf of Mexico. *Mar. Petroleum Geology* 26, 1190–1198. doi: 10.1016/j.marpetgeo.2008.07.001

Fraser, D. R. A., Gorman, A. R., Pecher, I. A., Crutchley, G. J., and Henrys, S. A. (2016). Gas hydrate accumulations related to focused fluid flow in the Pegasus Basin, southern Hikurangi Margin, New Zealand. *Mar. Petroleum Geology* 77, 399–408. doi: 10.1016/j.marpetgeo.2016.06.025

Fu, X., Jimenez-Martinez, J., Nguyen, T. P., Carey, J. W., Viswanathan, H., Cueto-Felgueroso, L., et al. (2020). Crustal fingering facilitates free-gas methane migration through the hydrate stability zone. *Proc. Natl. Acad. Sci.* 117, 202011064. doi: 10.1073/pnas.2011064117

Guo, X., Liu, K., He, S., Yang, Z., and Dong, T. (2016). Quantitative estimation of overpressure caused by gas generation and application to the Baiyun Depression in the Pearl River Mouth Basin, South China Sea. *Geofluids* 16, 129–148. doi: 10.1111/gfl.12140

He, M., Zhong, G., Liu, X., Liu, L., Shen, X., Wu, Z., et al. (2017). Rapid post-rift tectonic subsidence events in the Pearl River Mouth Basin, northern South China Sea margin. *J. Asian Earth Sci.* 147, 271–283. doi: 10.1016/j.jseaes.2017.07.024

Hillman, J. I. T., Cook, A. E., Daigle, H., Nole, M., Malinverno, A., Meazell, K., et al. (2017). Gas hydrate reservoirs and gas migration mechanisms in the Terrebonne Basin, Gulf of Mexico. *Mar. Petroleum Geology* 86, 1357–1373. doi: 10.1016/j.marpetgeo.2017.07.029

Hui, G., Li, S., Guo, L., Zhang, G., Gong, Y., Somerville, I. D., et al. (2016). Source and accumulation of gas hydrate in the northern margin of the South China Sea. *Mar. Petroleum Geology* 69, 127–145. doi: 10.1016/j.marpetgeo.2015.10.009

Jackson, C. A. L., and Rotevatn, A. (2013). 3D seismic analysis of the structure and evolution of a salt-influenced normal fault zone: A test of competing fault growth models. *J. Struct. Geology* 54, 215–234. doi: 10.1016/j.jsg.2013.06.012

Jin, J., Wang, X., Guo, Y., Li, J., Li, Y., Zhang, X., et al. (2020). Geological controls on the occurrence of recently formed highly concentrated gas hydrate accumulations in the Shenhu area, South China Sea. *Mar. Petroleum Geology* 116, 104294. doi: 10.1016/j.marpetgeo.2020.104294

Kong, L., Chen, H., Ping, H., Zhai, P., Liu, Y., and Zhu, J. (2018). Formation pressure modeling in the Baiyun Sag, northern South China Sea: Implications for petroleum exploration in deep-water areas. *Mar. Petroleum Geology* 97, 154–168. doi: 10.1016/j.marpetgeo.2018.07.004

Kuang, Z., Fang, Y., Liang, J., Lu, J.A., and Wang, L. (2018). Geomorphological-geological-geophysical signatures of high-flux fluid flows in the eastern Pearl River Mouth Basin and effects on gas hydrate accumulation. *Sci. China Earth Sci.* 61, 914–924. doi: 10.1007/s11430-017-9183-y

Kvenvolden, K. A. (1993). Gas hydrates—geological perspective and global change. *Rev. Geophysics* 31, 173–187. doi: 10.1029/93RG00268

Lai, H., Deng, Y., Yang, L., Liang, J., Dai, L., Li, L., et al. (2023). Origin of natural gas within the deep-sea uncompacted sediments of the Shenhu area, northern South China Sea: Geochemical and methanogenic cultivation results. *Mar. Petroleum Geology* 147, 106015. doi: 10.1016/j.marpetgeo.2022.106015

Lai, H., Qiu, H., Kuang, Z., Ren, J., Fang, Y., Liang, J., et al. (2022). Integrated signatures of secondary microbial gas within gas hydrate reservoirs: A case study in the Shenhu area, northern South China Sea. *Mar. Petroleum Geology* 136, 105486. doi: 10.1016/j.marpetgeo.2021.105486

Lei, C., Ren, J., Pei, J., Liu, B., Zuo, X., Liu, J., et al. (2021). Tectonics of the offshore Red River Fault recorded in the junction of the Yinggehai and Qiongdongnan Basins. *Sci. China Earth Sci.* 64, 1893–1908. doi: 10.1007/s11430-020-9796-2

Li, J.-f., Ye, J.-l., Qin, X.-w., Qiu, H.-j., Wu, N.-y., Lu, H.-l., et al. (2018). The first offshore natural gas hydrate production test in South China Sea. *China Geology* 1, 5–16. doi: 10.31035/cg2018003

Liang, J., Zhang, Z., Su, P., Sha, Z., and Yang, S. (2017). Evaluation of gas hydrate-bearing sediments below the conventional bottom-simulating reflection on the northern slope of the South China Sea. *Interpretation* 5, SM61–SM74. doi: 10.1190/INT-2016-0219.1

Liang, Q., Xiao, X., Zhao, J., Zhang, W., Li, Y., Wu, X., et al. (2022). Geochemistry and sources of hydrate-bound gas in the Shenhu area, northern south China sea: Insights from drilling and gas hydrate production tests. *J. Petroleum Sci. Eng.* 208, 109459. doi: 10.1016/j.petrol.2021.109459

Makogon, Y. F., Holditch, S. A., and Makogon, T. Y. (2007). Natural gas-hydrates — A potential energy source for the 21st Century. *J. Petroleum Sci. Eng.* 56, 14–31. doi: 10.1016/j.petrol.2005.10.009

Mi, L., Zhang, Z., Pang, X., Liu, J., Zhang, B., Zhao, Q., et al. (2018). Main controlling factors of hydrocarbon accumulation in Baiyun Sag at northern continental margin of South China Sea. *Petroleum Explor. Dev.* 45, 963–973. doi: 10.1016/S1876-3804(18)30100-9

Milkov, A. V. (2004). Global estimates of hydrate-bound gas in marine sediments: how much is really out there? *Earth-Science Rev.* 66, 183–197. doi: 10.1016/j.earscirev.2003.11.002

Milkov, A. V. (2005). Molecular and stable isotope compositions of natural gas hydrates: A revised global dataset and basic interpretations in the context of geological settings. *Organic Geochemistry* 36, 681–702. doi: 10.1016/j.orggeochem.2005.01.010

Milkov, A. V., and Etiope, G. (2018). Revised genetic diagrams for natural gases based on a global dataset of >20,000 samples. *Organic Geochemistry* 125, 109–120. doi: 10.1016/j.orggeochem.2018.09.002

Milkov, A. V., and Sassen, R. (2002). Economic geology of offshore gas hydrate accumulations and provinces. *Mar. Petroleum Geology* 19, 1–11. doi: 10.1016/S0264-8172(01)00047-2

Ouchi, H., Yamamoto, K., Akamine, K., Kano, S., Naiki, M., Tamaki, M., et al. (2021). Numerical history-matching of modeling and actual gas production behavior and causes of the discrepancy of the nankai trough gas-hydrate production test cases. *Energy Fuels* 36, 210–226. doi: 10.1021/acs.energyfuels.1c02931

Pang, X., Ren, J., Zheng, J., Liu, J., Yu, P., and Liu, B. (2018). Petroleum geology controlled by extensive detachment thinning of continental margin crust: A case study of Baiyun sag in the deep-water area of northern South China Sea. *Petroleum Explor. Dev.* 45, 29–42. doi: 10.1016/S1876-3804(18)30003-X

Portnov, A., Cook, A. E., and Vadakkepuliyambatta, S. (2021). Diverse gas composition controls the Moby-Dick gas hydrate system in the Gulf of Mexico. *Geology* 49, 1446–1451. doi: 10.1130/G49310.1

Qin, X.-w., Lu, J.-a., Lu, H.-l., Qiu, H.-j., Liang, J.-q., Kang, D.-j., et al. (2020). Coexistence of natural gas hydrate, free gas and water in the gas hydrate system in the Shenhu Area, South China Sea. *China Geology* 3, 210–220. doi: 10.31035/cg2020038

Qin, X.-w., Lu, C., Wang, P.-k., and Liang, Q.-y. (2022). Hydrate phase transition and seepage mechanism during natural gas hydrates production tests in the South China Sea: A review and prospect. *China Geology* 5, 201–217. doi: 10.31035/cg2022029

Ren, J., Cheng, C., Xiong, P., Kuang, Z., Liang, J., Lai, H., et al. (2022). Sand-rich gas hydrate and shallow gas systems in the Qiongdongnan Basin, northern South China Sea. *J. Petroleum Sci. Eng.* 215, 110630. doi: 10.1016/j.petrol.2022.110630

Santra, M., Flemings, P. B., Heidari, M., and You, K. (2022). Occurrence of high-saturation gas hydrate in a fault-compartmentalized anticline and the importance of seal, Green Canyon, abyssal northern Gulf of Mexico. *AAPG Bull.* 106, 981–1003. doi: 10.1306/08182120149

Sassen, R., Sweet, S. T., Milkov, A. V., DeFreitas, D. A., and Kennicutt, M. C. II (2001). Thermogenic vent gas and gas hydrate in the Gulf of Mexico slope: Is gas hydrate decomposition significant? *Geology* 29, 107–110. doi: 10.1130/0091-7613(2001)029<0107:TVGAGH>2.0.CO;2

Shi, H., He, M., Zhang, L., Yu, Q., Pang, X., Zhong, Z., et al. (2014). Hydrocarbon geology, accumulation pattern and the next exploration strategy in the eastern Pearl River Mouth basin. *China Offshore Oil Gas* 26, 11–22.

Sloan, E. D. (2003). Fundamental principles and applications of natural gas hydrates. *Nature* 426, 353–359. doi: 10.1038/nature02135

Slowey, N. C., Berti, D., and MacDonald, I. R. (2022). Salt-driven fluid venting chimneys at the base of the Sigsbee Escarpment, northwestern Gulf of Mexico. *Mar. Petroleum Geology* 135, 105396. doi: 10.1016/j.marpetgeo.2021.105396

Snodgrass, J. E., and Milkov, A. V. (2020). Web-based machine learning tool that determines the origin of natural gases. *Comput. Geosciences* 145, 104595. doi: 10.1016/j.cageo.2020.104595

Solomon, S., Qin, D., Manning, M., Averyt, K., and Marquis, M. (2007). *Climate change 2007-the physical science basis: Working group I contribution to the fourth assessment report of the IPCC* (Cambridge, United Kingdom and New York, NY, USA: Cambridge university press).

Su, M., Sha, Z., Zhang, C., Wang, H., Wu, N., Yang, R., et al. (2017). Types, characteristics and significances of migrating pathways of gas-bearing fluids in the shenhu area, northern continental slope of the south China sea. *Acta Geologica Sinica-English Edition* 91, 219–231. doi: 10.1111/1755-6724.13073

Sun, Z., Lin, J., Qiu, N., Jian, Z., Wang, P., Pang, X., et al. (2019). The role of magmatism in the thinning and breakup of the South China Sea continental margin: Special Topic: The South China Sea Ocean Drilling. *Natl. Sci. Rev.* 6, 871–876. doi: 10.1093/nsr/nwz116

Sun, L., Wang, X., He, M., Jin, J., Li, J., Li, Y., et al. (2020). Thermogenic gas controls high saturation gas hydrate distribution in the Pearl River Mouth Basin: Evidence from numerical modeling and seismic anomalies. *Ore Geology Rev.* 127, 103846. doi: 10.1016/j.oregeorev.2020.103846

Sun, Z., Zhihong, Z., Di, Z., Xiong, P., Chunju, H., Changmin, C., et al. (2008). Dynamics analysis of the Baiyun sag in the Pearl River Mouth Basin, north of the South China sea. *Acta Geologica Sinica-English Edition* 82, 73–83. doi: 10.1111/j.1755-6724.2008.tb00326.x

Wan, Z.-F., Zhang, W., Ma, C., Liang, J.-Q., Li, A., Meng, D.-J., et al. (2022). Dissociation of gas hydrates by hydrocarbon migration and accumulation-derived slope failures: An example from the South China Sea. *Geosci. Front.* 13, 101345. doi: 10.1016/j.gsf.2021.101345

Wang, D., Ning, F., Lu, J., Lu, H., Kang, D., Xie, Y., et al. (2021). Reservoir characteristics and critical influencing factors on gas hydrate accumulations in the Shenhu area, South China Sea. *Mar. Petroleum Geology* 133, 105238. doi: 10.1016/j.marpetgeo.2021.105238

Wei, J., Yang, L., Liang, Q., Liang, J., Lu, J., Zhang, W., et al. (2021). Geomechanical properties of gas hydrate-bearing sediments in Shenhu Area of the South China Sea. *Energy Rep.* 7, 8013–8020. doi: 10.1016/j.egyr.2021.05.063

Whiticar, M. J. (1999). Carbon and hydrogen isotope systematics of bacterial formation and oxidation of methane. *Chem. Geology* 161, 291–314. doi: 10.1016/S0009-2541(99)00092-3

Whiticar, M. J., Faber, E., and Schoell, M. (1986). Biogenic methane formation in marine and freshwater environments: CO2 reduction vs. acetate fermentation—Isotope evidence. *Geochimica Cosmochimica Acta* 50, 693–709. doi: 10.1016/0016-7037(86)90346-7

Wu, X., Pu, R., Zhang, G., Fan, X., Deng, D., and Li, B. (2018). Seismic interpretation of the diapiric structures and gas chimneys in the Liwan gas field, Pearl River Mouth Basin, northern South China Sea. *Interpretation* 6, T499–T519. doi: 10.1190/INT-2017-0129.1

Wu, N., Zhang, H., Yang, S., Zhang, G., Liang, J., Su, X., et al. (2011). Gas hydrate system of shenhu area, northern south China sea: geochemical results. *J. Geological Res* 370298. doi: 10.1155/2011/370298

Yang, S., Zhang, M., Liang, J., Lu, J., Zhang, Z., Holland, M., et al. (2015). Preliminary results of China's third gas hydrate drilling expedition: a critical step from discovery to development in the South China Sea. *Center Natural Gas Oil* 412, 386–7614.

Ye, J.-l., Qin, X.-w., Xie, W.-w., Lu, H.-l., Ma, B.-j., Qiu, H.-j., et al. (2020). The second natural gas hydrate production test in the South China Sea. *China Geology* 3, 197–209. doi: 10.31035/cg2020043

You, K., Flemings, P. B., Malinverno, A., Collett, T. S., and Darnell, K. (2019). Mechanisms of methane hydrate formation in geological systems. *Rev. Geophysics* 57, 1146–1196. doi: 10.1029/2018RG000638

Yu, Y.-S., Zhang, X., Liu, J.-W., Lee, Y., and Li, X.-S. (2021). Natural gas hydrate resources and hydrate technologies: a review and analysis of the associated energy and global warming challenges. *Energy Environ. Sci.* 14, 5611–5668. doi: 10.1039/D1EE02093E

Zhang, W., Liang, J., Wan, Z., Su, P., Huang, W., Wang, L., et al. (2020). Dynamic accumulation of gas hydrates associated with the channel-levee system in the Shenhu area, northern South China Sea. *Mar. Petroleum Geology* 117, 104354. doi: 10.1016/j.marpetgeo.2020.104354

Zhang, W., Liang, J., Wei, J., Su, P., Fang, Y., Guo, Y., et al. (2017). Accumulation features and mechanisms of high saturation natural gas hydrate in Shenhu Area, northern South China Sea. *Petroleum Explor. Dev.* 44, 708–719. doi: 10.1016/S1876-3804(17)30082-4

Zhang, W., Liang, J., Wei, J., Su, P., Lin, L., and Huang, W. (2019). Origin of natural gases and associated gas hydrates in the Shenhu area, northern South China Sea: Results from the China gas hydrate drilling expeditions. *J. Asian Earth Sci.* 183, 103953. doi: 10.1016/j.jseaes.2019.103953

Zhang, G., Qu, H., Jia, Q., Zhang, L., Yang, B., Chen, S., et al. (2021a). Passive continental margin segmentation of the marginal seas and its effect on hydrocarbon accumulation: A case study of the northern continental margin in South China Sea. *Mar. Petroleum Geology* 123, 104741. doi: 10.1016/j.marpetgeo.2020.104741

Zhang, B., Su, M., Chen, H., Liu, F., Zheng, W., Su, P., et al. (2023). How do fault systems and seafloor bathymetry influence the structure and distribution characteristics of gas chimneys? *Basin Res.* 35, 1718–1743. doi: 10.1111/bre.12770

Zhang, G., Wang, D., Lan, L., Liu, S., Su, L., Wang, L., et al. (2021b). The geological characteristics of the large- and medium-sized gas fields in the South China Sea. *Acta Oceanologica Sin.* 40, 1–12. doi: 10.1007/s13131-021-1754-x

Zhao, Z., Sun, Z., Sun, L., Wang, Z., and Sun, Z. (2016). Cenozoic tectonic subsidence in the Qiongdongnan Basin, northern South China Sea. *Basin Res.* 30, 269–288. doi: 10.1111/bre.12220

Zhou, D., Sun, Z., Liao, J., Zhao, Z., He, M., Wu, X., et al. (2009). Filling history and post-breakup acceleration of sedimentation in Baiyun Sag, deepwater northern South China Sea. *J. Earth Sci.* 20, 160–171. doi: 10.1007/s12583-009-0015-2

Zhu, W., Huang, B., Mi, L., Wilkins, R. W. T., Fu, N., and Xiao, X. (2009). Geochemistry, origin, and deep-water exploration potential of natural gases in the Pearl River Mouth and Qiongdongnan basins, South China Sea. *AAPG Bull.* 93, 741–761. doi: 10.1306/02170908099

Zhu, W., Shi, H., Huang, B., Zhong, K., and Huang, Y. (2021). Geology and geochemistry of large gas fields in the deepwater areas, continental margin basins of northern South China Sea. *Mar. Petroleum Geology* 126, 104901. doi: 10.1016/j.marpetgeo.2021.104901